MethodsX 7 (2020) 100833

Contents lists available at ScienceDirect

MethodsX

journal homepage: www.elsevier.com/locate/mex

Method Article

Visualization of small changes in the movement of cadaveric lumbar vertebrae of the human spine using speckle interferometry ☆

V. Janák*, L. Bartoněk, J. Keprt

Department of Experimental Physics, Palacky University Olomouc, Czechia

A B S T R A C T

Principles of coherent and non-coherent double exposure Speckle photography are presented with evaluation of shift changes in continuous and discrete areas. The aim of this work is to demonstrate that this computer method can be also employed in medical research. It may be transformed for the study of small deformations of the specimens of lumbar spines during applications of different physical strains.

- Incoherent computer speckle interferometry was used to visualize small changes in the assessment of lumbar spine surgical fixation.
- Vertebral movement is contactless monitored by two cheap CCD cameras and evaluated using computer technology.
- The results obtained were verified on a cadaveric sample of human spine.

A R T I C L E I N F O
Method name: Speckle interferometry
Keywords: Speckle interferometry, FFT, Lumbar spine, Strain gauge
Article history: Received 27 August 2019; Accepted 23 January 2020; Available online 21 February 2020

Specification Table

Subject Area:	∗ Medicine and Dentistry
More specific subject area:	Measurement of vertebra positions on lumbar spine by speckle interferometry
Method name:	Speckle interferometry
Resource availability:	In the article

☆ Suggested reviewers are not from the same institution as the author.

* Corresponding author.
E-mail addresses: holohlavek@centrum.cz, vladislav.janak@upol.cz (V. Janák).

https://doi.org/10.1016/j.mex.2020.100833

Introduction

Speckle interferometry or speckle photography is one of the most moderate-sensitivity measuring non-contact method that can be used in wide spectrum of technical and social praxis. This method may also be convenient in medicine, e.g., when the stiffness of cadaveric lumbar spines stabilized with several anterior interbody fusion devices is studied [9]. The information obtained proceeds a foundation for determining how methods of anterior lumbar fixation can maximize rigidity and promote development of body fusion. Until now the measurements of the deformations of the lumbar spines have been realized by contact-mechanical and electro-tensometrical methods [1,2]. To bring some new knowledge of this problem we propose to use the non-contact measuring method, e.g., the mentioned incoherent method of speckle-interferometry (double exposure speckle-photography) [3,4].

Methodology

Speckle patterns in laser light

When one observes or photographs a diffusely reflecting (or transmitting) object in laser light, its image has a granular appearance. It seems to be covered with fine, randomly distributed light and dark speckles. If one focuses in front of or behind the object, this speckle pattern is still visible. If the observer moves, the speckles appear to twinkle and move relative to the object. This phenomenon of speckle is inherent in the use of highly coherent light (laser light). The physical origin of speckle is quite simple. Each point on the object scatters some light to the observer. Because of its high coherence, the laser light scattered by one object points interferes with the light scattered by each of the other object point. When a detector such as a film, a camera or the retina of an eye is placed in the optical field, it observes a random pattern of interference field which is termed “speckle”. The randomness is caused by the surface roughness because the phase of light scattered will vary from point to point in proportion to the local surface height. For our purposes the most important statistical characteristics of laser speckle is its size. In most cases a diffusely reflecting or transmitting object ABC will be viewed through a lens L or imaging system, as indicated in Fig. 1.

To estimate the speckle size in the image plane of the lens L, the distance of which from the lens is z, we need only to treat the disk enclosed by the pupil of the lens as a uniformly illuminated diffuse surface. If the diameter of the lens pupil is D an analysis of this problem [3,4] leads to the expression

$$b_s \doteq 1.22\left(\frac{\lambda z}{D}\right), \tag{1}$$

Where b_s is considered as a typical speckle width in the image plane and λ is the wavelength of the laser light. If the imaging system is focused on a relatively distant plane,

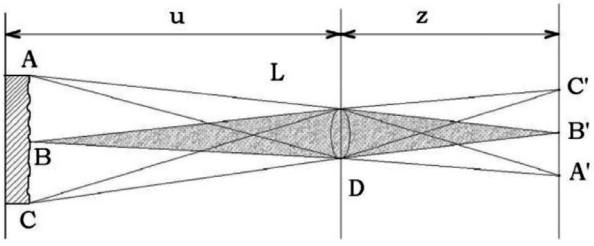

Fig. 1. Surface with randomly scattering laser light imaged by lens L.

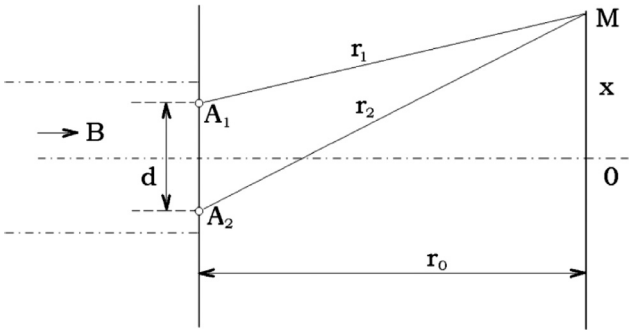

Fig. 2. Experimental set up to form Young s fringes.

$z \doteq f$ =focal length of the lens, then

$$b_s \doteq 1.22\lambda\left(\frac{f}{D}\right) \tag{2}$$

wheref/D is the f number of the lens. The diameter of a lens of typical imaging systems vary from about $f/1.4$ to $f/32$. If the speckle pattern is formed by imaging scattered He-Ne laser light ($\lambda = 633\text{nm}$), the corresponding speckle size varies from $1\mu\text{m}$ to $24\mu\text{m}$.

Young's fringes

If we consider a simple opaque screen in which two small holes A_1 and A_2 separated by a distance $d$have been cut, then if this screen is illuminated by a laser beam B, the light diffracted by two holes forms an interference pattern which can be observed on a screen placed some distance r_0 away (Fig. 2).

Let us study the interference pattern on this screen in the point Mwhich has the vertical coordinate $x$from the origin 0. The distances of the point $M$from the holes A_1 and A_2 are r_1 and r_2, respectively. The phase difference φ in the point M can be expressed in the form [5]

$$\varphi = \frac{2\pi}{\lambda}(r_2 - r_1) \tag{3}$$

and the interference pattern characterized through the intensity Ican be written by the relation

$$I = I_1 + I_2 + 2\sqrt{I_1 I_2}\cos\varphi, \tag{4}$$

where I_1 and I_2 are the light intensities generated from the holes A_1 and A_2. If $I_1 = I_2 = I_0$, then the simplified form of the relation (4) can be derived [6].

$$I = 2I_0(1 + \cos\varphi). \tag{5}$$

From this form we can see that the Youngś pattern is formed by light and dark fringes (Fig. 3) which spacing p(period) depends on the path difference

$$\Delta r = r_2 - r_1. \tag{6}$$

From Fig. 2 we can write

$$r_1^2 = r_0^2 + \left(x - \frac{d}{2}\right)^2 \tag{7}$$

and

$$r_2^2 = r_0^2 + \left(x + \frac{d}{2}\right)^2. \tag{8}$$

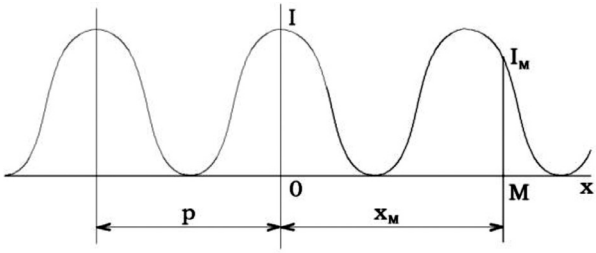

Fig. 3. Intensity distribution of Young's fringes.

Then equation

$$r_2^2 - r_1^2 = (r_2 - r_1).(r_2 + r_1) = 2xd \tag{9}$$

can be rearranged as

$$\Delta r = \frac{xd}{r_0} \tag{10}$$

because r_1, r_2, r_0 are much greater than x and d. The Young's fringes become then the final form [5]

$$I = 2I_0\left(1 + \cos\frac{2\pi}{\lambda}\cdot\frac{d}{r_0}.x\right) \tag{11}$$

with the spacing p(or spatial frequency ν)

$$p = \frac{1}{\nu} = \frac{\lambda r_0}{d}. \tag{12}$$

Speckle photography

Speckle photography is a technique for making moderate-sensitivity measurements of in-plane translation, strain, rotation, and vibration. It can also be used to measure out-of-plane rotation (tilt). Its principal attractions are the simplicity of the optical system and the relative simplicity of displaying and interpreting the results. The sensitivity of the method can be varied during the readout process. To introduce the basic concepts of speckle photography we consider the arrangement on Fig. 1.

The system for measuring in-plane translation supposes that an image of the object surface is formed in the detection of a plane by lens of diameter D. The object distance $u$and image distance z are related by Eq. (13) where β is the magnification of the imaging system.

$$\beta = \frac{z}{u} \tag{13}$$

From the discussion in the second chapter we know that the image formed in the recording plane is modulated by a random pattern of speckles having a characteristic size b_s given by Eq. (1). If the object translates vertically by an amount d_1, the relative phase of the light in each of the various rays that contribute to the formation of each speckle will be unchanged.

Hence the speckle pattern will be simply translated as a whole in the image by the amount $d = \beta d_1$, where β is the lateral magnification of the imaging lens given by Eq. (13). The translation of the speckle pattern for these in-plane motions is independent on the angle of illumination of the laser beam [3,4]. To measure the in-plane translation of the object surface (in case of continuous recording), the film (optical detector) is exposed twice-one before the translation, and once after it.

If we assume that the magnitude d of the in film translation is greater than the speckle size b_s, the developed film will contain a pair of identical speckle patterns separated by a distance d. Naturally, the separation distance d of each speckle pair can be measured directly by microscopic examination

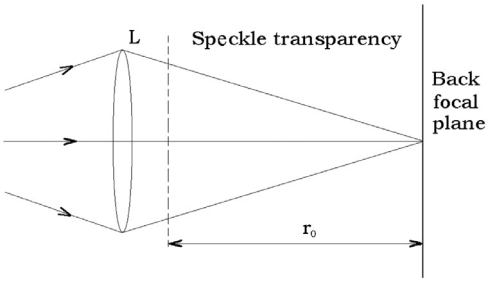

Fig. 4. Processing system for two-exposure speckle photography.

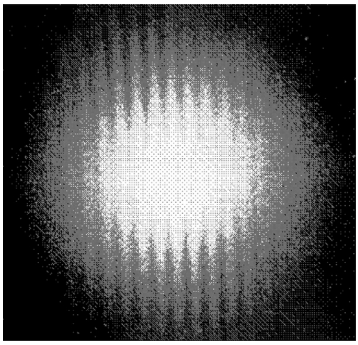

Fig. 5. Fringe pattern formed in back focal plane by processing system in Fig. 4.

of the film, but by simple coherent optical processing of the developed film, the displacement can be displayed in the form of a fringe pattern.

The film is placed in a converging spherical wave of laser light formed by lens, as shown in Fig. 4.

The irradiant distribution in the back focal plane of the lens consists of a bright central spot surrounded by a speckle pattern modulated by cosinusoidal fringes, as shown in Fig. 5. This is due to the fluctuation of the classical coherent speckle.

The bright central spot is formed by un-diffracted light transmitted by the transparency. The modulated speckle pattern is generated by light diffracted by the speckle pattern recorded in the transparency. The cosinusoidal fringes are formed because each pair of corresponding speckles acts as a pair of identical sources of coherent light which form Young's fringes. Since all speckle pairs are separated by the same distance d, all of the Young's fringes overlap to form the pattern shown in Fig. 5. Interpretation of the fringes is straight forward. First, their orientation is normal to the in-plane translation. Second, the magnitude of the translation on the film can be determined by applying Eq. (12).

If we use for the film exposure the arrangement in Fig. 6 (see Fig. 1), then the magnitude d_1 of the object translation is given by Eq. (13), where d means the speckle translation in the film. Then

$$d = \beta d_1 \tag{14}$$

and with a session (12)

$$d_1 = \frac{\lambda}{\beta}\frac{r_0}{p} \tag{15}$$

where p is the Young's fringes spacing and r_0 is the distance of the back focal plain, from the plane of the film. For illustration let us take the spacing $p = 1\text{cm} = 10$ mm in the back focal plane and the distance $r_0 = 1\text{m} = 10^3\text{mm}$ (Fig. 4). For the simplicity we can consider $\lambda \doteq 0.5\mu\text{m} = 5.10^{-4}\text{mm}$. Then

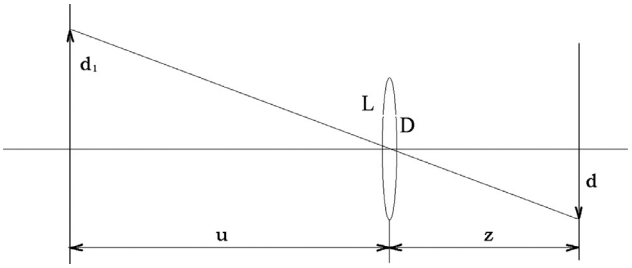

Fig. 6. Geometrical arrangement of the imaging system.

the separation distance *d*on the film is by Eq. (12)

$$d = \lambda \frac{r_0}{p} = 5.10^{-4} \frac{10^3}{10} = 0.05\text{mm} \tag{16}$$

If the object distance $u = 2\text{m} = 2.10^3\text{mm}$ and the distance $z = 20\text{cm} = 2.10^2\text{mm}$, then using result (16) we get

$$d_1 = \frac{u}{z} d = \frac{2.10^3}{2.10^2} 0.05 = 0.5\,\text{mm}. \tag{17}$$

If we use in an optical system $f \doteq z \doteq 50\text{mm}$ than the spacing $p = 10\text{mm}$ appoints a deformation $d = 2\text{mm}$. This example shows the high flexibility of the measuring method.

Double - exposure speckle photography (continuous display) in laser light

To show the possibility of the lumbar spines measurement by double - exposure speckle photography we designed and constructed a model of human cadaveric lumbar spines. Four wooden cylinders of the diameter 6 cm and the height 4cm were connected with four rubber cylinders (tablets) of the diameter 3cm and the high 1 cm by a metal stick and screwed into a magnetic holder standing on the metal desk (table). The rubber tablets were put between each couple of wooden cylinders. On this model we have simulated the most important strains connected with the loads of lumbar spines. That means, we have to measure axial compression, axial torsion and lateral bending (flexion-extension) during the simultaneous loads of the model. The model was illuminated by the light of He-Ne laser $\lambda = 633\text{nm}$ and photographed by a lens of diameter $D = 30\text{mm}$. The object distance $u = 2\text{m}$, the image distance $z = 20\text{cm}$. The considered speckle width b_s in the image plane given by Eq. (1) $b_s = 5\mu\text{m} = 0.005\text{mm}$. That is why the recording material had to have high resolving power. The holographic film 24*x*36mm Agfa Gevared 10E75 was used for the exposure. The developed film was put into narrow converging laser beam. Then the image of each wooden cylinder diffracted the light separately. The Young's fringes characterized by the direction and by spacing period *p*enabled to determine the direction and the quality of deformation, e.g., the shift of the wooden cylinder. Simulation of axial compression was practiced by 15 N compressive load (Fig. 7). Axial torsion we realized through a small turn of the screw-key (Fig. 8) and the tilt (bending, flexion, extension) by a 20 cm long bar loaded on the end with 2 N weight (Fig. 9).

The mentioned strains and corresponding deformations are presented in Fig. 10. The direction and the quantity of displacement of separated parts of the model are clear from the system of Young's fringes on the right side of Fig. 10. The signs *L*2,*L*3,*L*4,*L*5 determine corresponding wooden cylinders that correlate to single lumbar spines (vertebras).

Fast Fourier transformation method in discrete domain

The results obtained, see Fig. 10, can also be obtained by digital recording (CCD camera) of the initial and displaced field produced by laser light, their sum and computer computation of their spectrum by means of discrete Fourier transform.

Fig. 7. Simulation of bending.

Fig. 8. Simulation of axial compression.

Fig. 9. Simulation of axial torsion.

The Fourier Transform is defined in the continuous domain as

$$F(u,v) = \int_{-\infty}^{\infty} f(x,y) e^{-j2\pi(xu+yv)} dxdy \tag{18}$$

where $f(x, y)$ is the light intensity of the point (x, y), and (u, v) are the horizontal and vertical spatial frequencies. The Fourier transform assigns a complex number to each set (u, v). Inversely, a Fourier Transform $F(u, v)$ can be transformed into a spatial image $f(x, y)$ of resolution NM using the following formula:

$$f(x,y) = \sum_{u=0}^{N-1} \sum_{v=0}^{M-1} F(u,v) e^{j2\pi\left(\frac{ux}{N}+\frac{vy}{M}\right)}. \tag{19}$$

In the discrete domain, the Fourier Transform is calculated with an efficient algorithm called the Fast Fourier Transform (FFT). It can be written in the form

$$F(u,v) = \frac{1}{NM} \sum_{x=0}^{N-1} \sum_{y=0}^{M-1} f(x,y) e^{-j2\pi\left(\frac{ux}{N}+\frac{vy}{M}\right)} \tag{20}$$

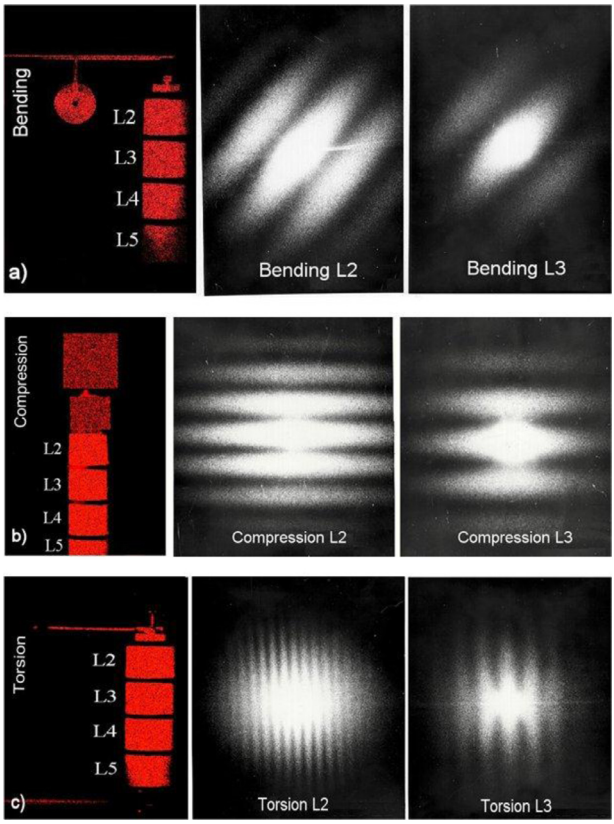

Fig. 10. By double exposure laser speckle photography demonstrated measurements; a) bending; b) compression; c) torsion.

where N x M is the size of the image $f(x, y)$. Derived calculation was programmed by the help of development environment NI LabView according to [10]. Fig. 11 shows the movements of the fields with laser speckle and its spectrum obtained by discrete Fourier transform.

It is clear from Fig. 11c that the displacement of the field corresponds to low frequencies. To ensure that the period of the strips is read, it is necessary to suppress the high frequencies that occur when recording coherent laser images.

Simulation of interference image

For our simple case of tracking shift changes, the speckle field can be simulated by a computer random number generator (Fig. 12).

The advantage of this solution is the possibility of high frequency suppression. The required grain size of the spot may be determined by the standard deviation σ derived from the histogram and the cumulative histogram [13], where:

Mean value M is selective (arithmetic) mean (estimate of medium value) calculated according to the formula:

$$M = \frac{1}{n}\sum_{i=0}^{255} i.h(i). \tag{21}$$

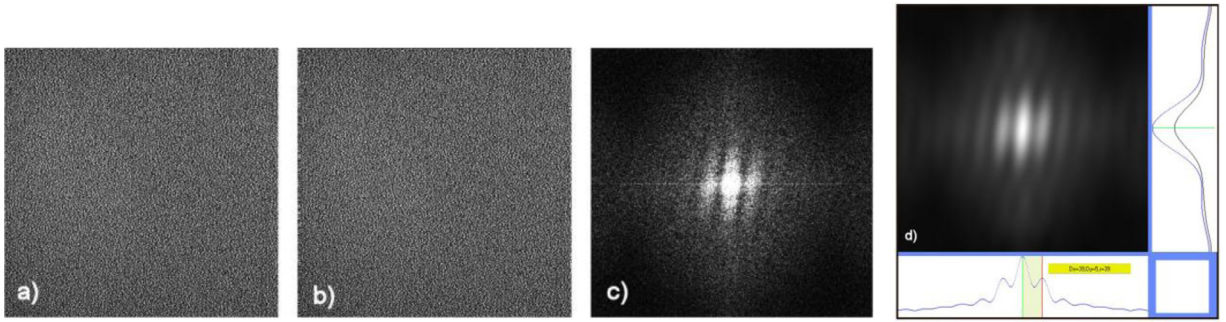

Fig. 11. Record of laser speckle fields; (a) Initial state; (b) Shifted field; (c) FT of sum of records. (d) Fourier spectrum after application of low-pass filter.

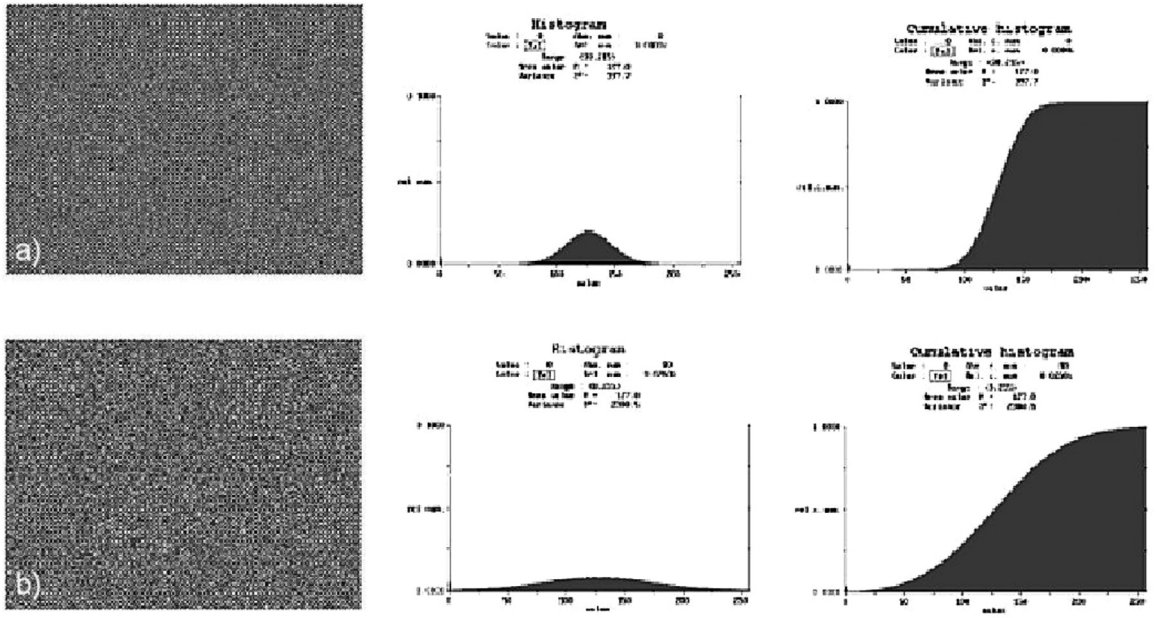

Fig. 12. Simulated graphics files $M(\mu) = 127$, (a) $\sigma = 20$ and (b) $\sigma = 50$.

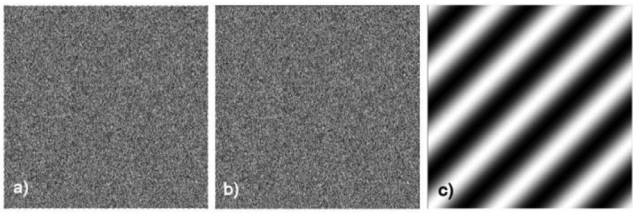

Fig. 13. Simulated speckle field; (a) Initial state; (b) Shifted field $x = 2$ pixel, $y = 4$ pixel; (c) 2D FFT of sum (a), (b) field.

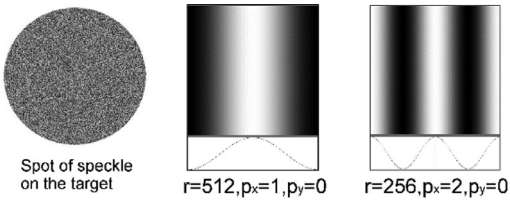

p image distance	1	2	3	5	10	15	20	40	60
r period	512	256	171	103	51	34	26	13	8

Fig. 14. The example of the interferograms and size periods (p_x and p_y~ shift in x and y axis, r ~ equivalent period).

Variance S^2 - sample variance (variance estimate D $\approx$ deviation) is calculated according to the formula:

$$S^2 = \frac{1}{n}\sum_{i=0}^{255}(i-M)^2.h(i). \tag{22}$$

Standard deviation

$$\sigma(x) = \sqrt{D(x)}, \tag{23}$$

n indicates the number of all pixels in the image and $h(i)$ an absolute frequency of class i. The depth of one pixel of intensity is 1B ($2^8 = 256$).

Fig. 13(a) shows a simulated initialization spot pattern generated by a computer random number generator. Standard deviation $\sigma = 20$. Fig. 13(b) displays speckled field from Fig. 13(a) shifted in the x-axis = 2 pixels and $y = 4$ pixels. Fig. 13(c) then shows the calculated Fourier 2D spectrum of the sum of the fields of Fig. 13(a) and (b).

To measure the displacement of the individual vertebrae, the simulated speckle fields were printed on aluminum circular targets that were attached to the spinal vertebrae of interest.

Fig. 14 shows examples of the dependence of the distance r of two neighbor fringes in the Fourier spectrum on the distance p of the number of pixels in the image file [10–12]. The p and r values are expressed in pixels.

From Fig. 15 is clear that the image distance p is in indirect proportion to the period r of the Fourier spectrum. The curve (line 1) in Fig. 15 can be approximated by the line 2 (hyperbola).

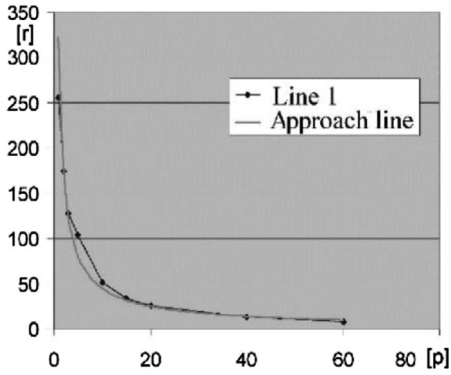

Fig. 15. The dependence of the spectral period r on the image distance p.

Mathematical expression is than in the form

$$p = \frac{c}{r}, \tag{24}$$

where value c shows constant, which can be determined by a specific measurement from Figs. 14 and 15 by relation (20).

$$c = pxr \approx 512. \tag{25}$$

The empirical relation for dependence between distance point in graphics file and distance neighbor fringes in the Fourier spectrum is then

$$p = \frac{512}{r}. \tag{26}$$

For example, with knowledge of Eq. (26) and size period $r = 128$ in interferential picture we can simply determine that size displacement $p = \frac{512}{128} = 4$pixels.

Eq. (26) does not represent the complete accuracy of the whole system. Total accuracy is discussed in [8].

The study of the movement of the individual spine parts was performed by observing round aluminum targets with printed simulated speckle field from two mutually perpendicular directions using two Vision Marlin F131B CCD cameras from Allied Technology and AVENIR SW2514 25.0 mm lenses (Fig. 16). The optical signal was fed to the computer memories for further processing using an analogue digital unit.

Experimental results

Application of non-coherent speckle interferometry in BS-II experimental equipment

To ensure repeatability and statistical processing, a second-generation computer system BS-II was designed (Fig. 16), [7,8]. The basis of the machine chassis is a massive metal plate, standing on four metal legs (Fig. 17) including mounting holes for individual components. The system of levers and drawers passes through the center of the structure which together with the clamping system and four step-motors ensure movement of the sample during the measurements.

The sample was completed with two aluminum jigs which, by means of self-tapping hexagon, bolt it fixed firmly in both axial and radial directions with L1 and L5.

The mechanically fixed sample is inserted into the BS-II device and is connected to next parts of the device that are adapted to each type of sample load by other mechanical elements.

In the case of biomechanical measurement of a cadaveric sample of the human spine, round discs with simulated spots were attached to the vertebrae of interest (Fig. 18).

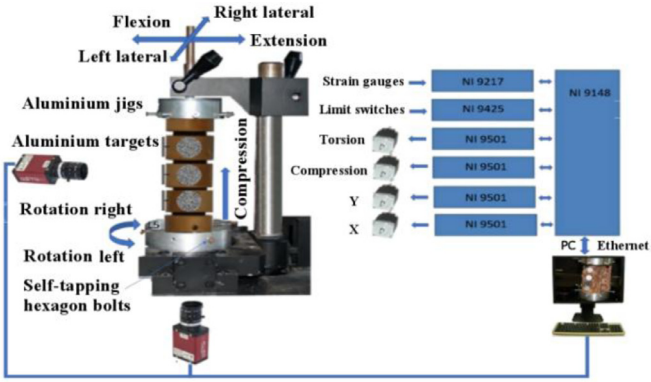

Fig. 16. Block diagram of BS-II.

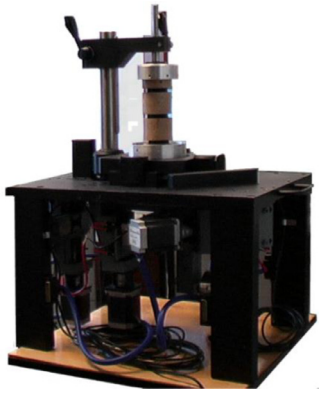

Fig. 17. Designed BS-II.

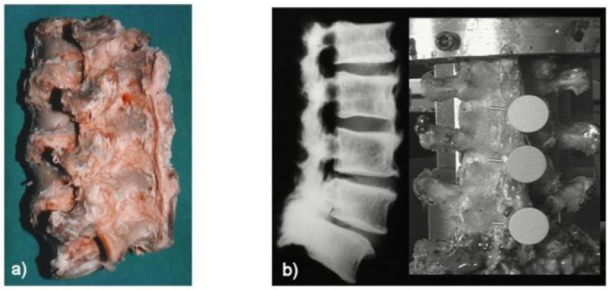

Fig. 18. (a) A pattern of a dead human lumbar spine; (b) with round targets covered with generated speckle patterns.

The untreated (intact) spine sample was mechanically circularly shifted at 0.1 Hz several times prior to measurement.

During sample acquisition, images from both cameras were saved from each position for bend (front bend), elongation (back bend), right and left side bend (lateral bend), left and right axial twist (rotation), and axial compression (pressure). The direction and displacement of the individual components was determined by the band of the calculated 2D FT spectrum. You see in Figs. 19–21.

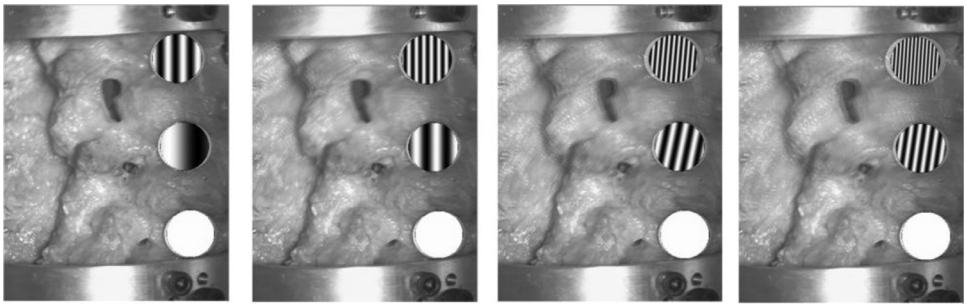

Fig. 19. Movements of L2, L3 and L4 by calculated Fourier transformation in the case of bending.

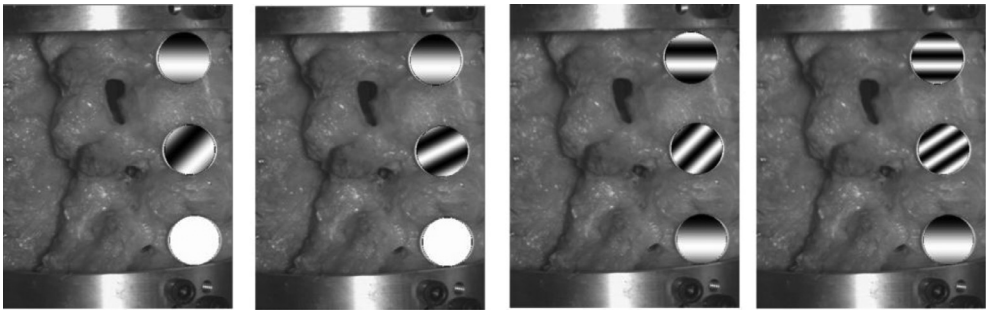

Fig. 20. Movements of L2, L3 and L4 by calculated Fourier transformation in the case of compression.

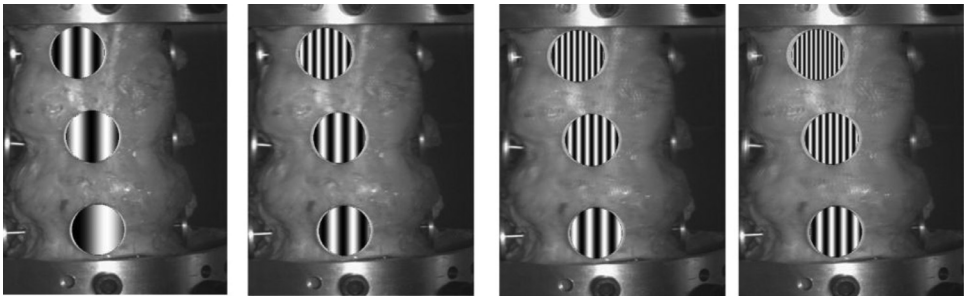

Fig. 21. Movements of L2, L3 and L4 by calculated Fourier transformation in the case of torsion.

The resulting measurement images visualize the movement of individual vertebrae of the spine under load. The movement of the monitored parts is proportional to the number of interference strips and is perpendicular to them. The main advantage, however, is that the speckle field image information captured by the cameras allows a cheap camera to achieve greater accuracy in determining changes than in direct tracking.

Conclusion

It was demonstrated that the non-coherent speckle interferometry can be used for the study of separated deformations of the human cadaveric specimens sequentially loaded in axial compression and torsion, flexion and extension, and lateral bending. The very simple theory of the speckle double-exposure method enables the simple evaluation of the deformations during the mentioned strains. We

have designed a special BS-II device enabling to evaluate before and after the application of various fixation methods for measuring the amount of cadaverous specimen load and corresponding amount of deformation. This may be a very important contribution to modern medical practice.

Acknowledgments

The work was further supported by the projects AFNet (CZ. 1.07/2.4.00/17. 0014) and IGA 2017, Palacky University in Olomouc and Proof of Concept UP PoC_0802, 909710012/90. The bio-material used for scientific purposes originates from the collection of the Institute of Normal Anatomy and has been supplied and used with the consent of the deceased in accordance with the provisions of Article 88 (1) (d) (6) 372/2011 on health services and the conditions of its provider.

Declaration of Competing Interests

The authors have no conflict of interests to disclose.

References

[1] D.S. Brodke, J.C. Dick, D.N. Kunz, R. McCabe, T.A. Zdeblic, Posterior lumbar interbody fusion, Spine 22 (N. 1) (1997) 26–31.
[2] Glazer, P.A., Collio, O., Klisch, S.M., Bradford, D.S., Bueff, H.N., Lotz, J.C.: Biomechanical Analysis of Multilevel Fixation Methods in the Lumbar Spine, 22, N. 2 (1997), 171–187.
[3] E. Archbold, J. Burch, A.E. M., Ennos, Recording of in-plane surface displacement by double - exposure speckle photography, Opt. Acta 17 (1970) 883–898.
[4] K.A. Stetson, A review of speckle photography and interferometry, Opt. Eng. 14 (1975) 482–489.
[5] J. Keprt, Elementary theory of interference and coherence, Acta Univ. Palacki. Olomouc. Fac. Rer. Nat. Phys. 37 (1972) 245–260.
[6] J. Keprt, L. Bartoněk, Measurement of small deformations by laser speckle interferometry, Acta Univ. Palacki. Olomouc. Fac. Rer. Nat. Phys. 38 (1999) 115–125.
[7] L. Bartoněk, J. Keprt, J. Charamza, L. Hrabálek, Computer aided measurement of biomechanical characteristic of cadaverous lumbar spines, Cent. Eur. J. Phys. 2 (3) (2004) 504–510.
[8] L. Bartoněk, V. Janak, J. Keprt, Automatic device for measuring biomechanical properties of cadaveric lumbar vertebrae of the human spine, SPIE 10142 (20) (2016) UNSP 1014217, doi:10.1117/12.2262461.
[9] M. Manohar, Panjabi, The stabilizing system of the spine. Part II. Neutral zone and instability hypothesis, J. Spinal Disord. 5 (4) (1992) 390–397 Raven Press, Ltd., New York.
[10] Z. Peng, T.B. Kirk, Two-dimensional fast Fourier transform and power spectrum for wear particle analysis, Tribol. Int. 30 (8) (1997) 583–590.
[11] M. Šonka, V. Hlaváč, R. Boyle, Image Processing, Analysis, and Machine Vision, Thomson Learning, Toronto, 1972.
[12] J. Túma, Processing of Signals Obtained from Mechanical Systems Using FFT, Communication Technology Praha, 1997 ISBN 80-901936-1-7.
[13] M. Druckmüller, P. Heriban, Scientific Image Analyzer DIPS 5.0, SOFO, Brno 1996.